Atmos. Chem. Phys., 8, 5061–5075, 2008
www.atmos-chem-phys.net/8/5061/2008/

Atmospheric Chemistry and Physics

Pressure broadening in the $2\nu_3$ band of methane and its implication on atmospheric retrievals

C. Frankenberg[1], T. Warneke[2], A. Butz[1], I. Aben[1], F. Hase[3], P. Spietz[2], and L. R. Brown[4]

[1]Netherlands Institute for Space Research, Sorbonnelaan 2, 3584 CA Utrecht, The Netherlands
[2]Institute of Environmental Physics, Otto-Hahn-Allee 1, 28359 Bremen, Germany
[3]Institut für Meteorologie und Klimaforschung, Forschungszentrum Karlsruhe, 76021 Karlsruhe, Germany
[4]Jet Propulsion Laboratory, California Institute of Technology, 4800 Oak Grove Drive, Pasadena, CA 91109, USA

Received: 26 March 2008 – Published in Atmos. Chem. Phys. Discuss.: 29 May 2008
Revised: 4 August 2008 – Accepted: 11 August 2008 – Published: 1 September 2008

Abstract. N_2-broadened half widths and pressure shifts were obtained for transitions in the $2\nu_3$ methane band. Laboratory measurements recorded at 0.011 cm^{-1} resolution with a Bruker 120 HR Fouriertransform spectrometer were analysed from 5860 to 6185 cm^{-1}. A 140 cm gas cell was filled with methane at room temperature and N_2 as foreign gas at pressures ranging from 125 to 900 hPa. A multispectrum nonlinear constrained least squares approach based on Optimal Estimation was applied to derive the spectroscopic parameters by simultaneously fitting laboratory spectra at different ambient pressures assuming a Voigt line-shape. At room temperature, the half widths ranged between 0.030 and 0.071 cm^{-1} atm^{-1}, and the pressure shifts varied from –0.002 to –0.025 cm^{-1} atm^{-1} for transitions up to J''=10. Especially for higher rotational levels, we find systematically narrower lines than HITRAN predicts. The Q and R branch of the new set of spectroscopic parameters is further tested with ground based direct sun Fourier transform infrared (FTIR) measurements where systematic fit residuals reduce by about a factor of 3–4. We report the implication of those differences on atmospheric methane measurements using high-resolution ground based FTIR measurements as well as low-resolution spectra from the SCanning Imaging Absorption SpectroMeter for Atmospheric ChartographY (SCIAMACHY) instrument onboard ENVISAT. We find that for SCIAMACHY, a latitudinal and seasonally varying bias of about 1% can be introduced by erroneous broadening parameters.

Correspondence to: C. Frankenberg
(c.frankenberg@sron.nl)

1 Introduction

Methane (CH_4) is, after carbon dioxide, the second most important anthropogenic greenhouse gas, directly contributing 0.48 W/m^2 to the total anthropogenic radiative forcing of 2.63 W/m^2 by well-mixed greenhouse gases (IPCC, 2007). Although the global annual source strength of methane (550±50 Tg/year) is comparatively well constrained, considerable uncertainties still exist in regard to the partitioning amongst sources and their spatial and temporal distribution.

SCIAMACHY (SCanning Imaging Absorption SpectroMeter for Atmospheric ChartographY) onboard ENVISAT provides the unique opportunity to monitor methane globally with high sensitivity for the entire atmospheric column, including the surface layers where sources are located. Results obtained so far (Frankenberg et al., 2005a, 2006; Bergamaschi et al., 2007; Buchwitz et al., 2006) underline the potential of SCIAMACHY to detect local and regional methane sources. However, there are indications for systematic biases as detailed in Frankenberg et al. (2006) and Bergamaschi et al. (2007). Hence, we want to investigate whether spectroscopic uncertainties can be the cause of observed retrieval biases.

Most research groups (Frankenberg et al., 2006; Buchwitz et al., 2006; Schneising et al., 2008) perform methane retrievals from SCIAMACHY in a microwindow in channel 6, ranging from 5983 to 6138 cm^{-1} (1629–1671 nm). This spectral range comprises the strong Q and R branches of the $2\nu_3$ methane band as well as numerous weaker lines for which the quantum assignments are unknown. Figure 1 depicts one of the recorded FTS (Fourier transform spectrometer) spectra as well as a SCIAMACHY spectrum over the Sahara. One can clearly identify the congested Q-branch at

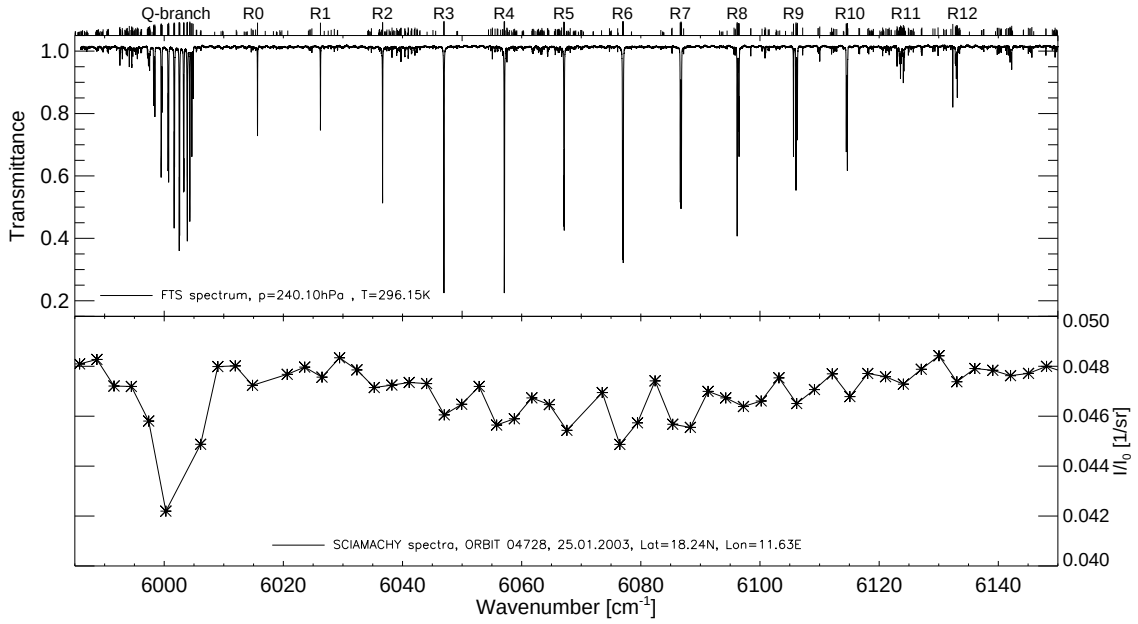

Fig. 1. Example of a recorded FTS methane transmission spectrum at 240.1 hPa (top) and a SCIAMACHY reflectance spectrum over the Sahara (bottom). On top of the plot, a stick spectrum of methane in logarithmic scale is depicted to indicate line positions and strengths. In addition, the attribution to Q and R-branch transitions in the $2\nu_3$ band is given. Please note that the SCIAMACHY spectrum is not absolute-radiometric calibrated, so only relative variations should be considered. The major absorber in the SCIAMACHY spectrum is CH_4 but smaller absorptions by CO_2 and H_2O are also present.

about 6000 cm^{-1} as well as the more widely spaced transitions in the R branch at higher wavenumbers. The spectral resolution of SCIAMACHY in this channel is relatively poor with a FWHM (Full width at half maximum) of 1.33 nm ($\approx$4.8 cm^{-1}), sampling the entire Q-branch with a mere 3-4 detector pixels.

Thus, individual lines are not resolved, so that incorrect line-shapes do not necessarily result in systematic retrieval residuals. However, if absorptions are strong, the line-shape and pressure shifts govern the sensitivity of the retrievals with respect to trace gas perturbations (Frankenberg et al., 2005b) as broader lines absorb more efficiently. This can cause systematic biases that change with the degree of saturation of the absorption lines, i.e. also with viewing geometry. Washenfelder et al. (2003) already found systematic biases in methane total columns retrieved from ground-based FTIR measurements in the P-branch of the $2\nu_3$ band.

For methane, the HITRAN 2004 linelist (Rothman et al., 2005; Brown et al., 2003) in this region is mainly based on empirical line positions and intensities of Margolis (1988, 1990). Measurements were performed at low pressures, thus only estimated broadening coefficients from limited measurements were adopted. The widths ranged from 0.054 to 0.066 cm^{-1} atm^{-1} at 296 K for J″=0 to 10, and transitions of the same lower state energy were given the same widths regardless of rotational symmetry (A,F,E). All air-broadened pressure shifts were set to a constant –0.008 cm^{-1} atm^{-1}. Margolis (1990) originally provided calculated ground state energies for assigned $2\nu_3$ transitions and empirical lower state energies for many of the unassigned features, but in HITRAN 2004, all the empirical values were replaced by –1, leaving lower state energies only for the assigned transitions in the $2\nu_3$ band.

Methane exhibits a complex spectrum with each J rotational level split into tetrahedal components and an ordering index. At temperatures encountered in the atmosphere, the multiplets are strongly blended even if only Doppler broadened. This renders the accurate measurement of individual broadening coefficients and pressure shifts difficult. To date, only few transitions in the $2\nu_3$ band have been studied with respect to pressure broadening. Gharavi and Buckley (2005) report broadening coefficients and line strengths for the R3 and R4 multiplets, while Kapitanov et al. (2007) report broadening and pressure shifts for the R3 triplet. To complicate matters, numerous studies observe collisional-narrowing and line-mixing effects in methane spectra. Dufour et al. (2003) report Dicke-narrowing for the $2\nu_3$ R0 transition and in addition line mixing effects for the R3 multiplet. Pine (1992, 1997); Pine and Gabard (2003) and Predoi-Cross et al. (2007) report Dicke narrowing and line mixing effects in transitions at about 3000 and 4350 cm^{-1}. Mondelain et al. (2007) show how collisional narrowing and line-mixing in the P9 manifold of the ν_3 band impact atmospheric profile retrievals by up to 7% (see also Mondelain et al. (2008) for

a discussion on the effect of the temperature dependence of the broadening coefficient). In this study, we neglect those intricacies of methane spectroscopy but follow a pragmatic approach to determine an updated set of effective methane spectroscopic parameters with focus on pressure-broadening.

The paper is structured as follows: Sect. 2 describes the experimental setup, followed by a description of the applied inverse method in Sect. 3. Derived spectroscopic parameters are presented and discussed in Sect. 4 and the impact on atmospheric retrievals is shown in Sect. 5. Conclusions are drawn in Sect. 6.

2 Experimental setup

Laboratory spectra were recorded over the 5600–6300 cm^{-1} spectral range with a Bruker IFS 120 HR FTS located at the Institute of Environmental Physics of the University of Bremen. All spectra were obtained using a tungsten lamp as the infrared source, a 1.7 mm input aperture at the entrance of the FTS, a CaF_2 beamsplitter and a liquid nitrogen cooled InSb detector. An optical filter was used to reduce the bandpass. This optical filter was not wedged, which resulted in a sinusoidal structure in the continuum. The gas mixtures were introduced in a 140 cm cell. For thermal stabilization and insulation the cell body is enclosed by 2 coaxial quartz jackets. The inner one is temperature stabilized by a flow of ethanol from a thermostatic bath. The outer one is evacuated for thermal insulation. Windows at the front and back end of the cell are made of CaF_2. The cell was located behind the interferometer and the light passed twice through the cell before being detected.

Transmission spectra were calculated by dividing sample spectra (resolution=0.011 cm^{-1}) by the spectra obtained for the evacuated cell (resolution=0.1 cm^{-1}). Twenty-five interferograms were co-added for the calculation of the spectra, resulting in a signal-to-noise of about 200 for the transmission spectra.

To achieve a uniform and constant methane mixing ratio in the cell, it was first filled with N_2, then with methane and finally with N_2. During the measurements the pressure in the cell remained stable to within 0.6% or better. Table 1 gives an overview of measurement conditions and measured spectra applied in this study. All spectra were recorded consecutively on the same day, and we assumed the internal calibration of the FTS was unchanged during that time. The pressure in the absorption vessel was measured with two independent capacitive pressure transducers of 500 hPa and 1000 hPa maximum range (MKS Baratron).

3 Data analysis

We applied a nonlinear fitting approach to derive the spectral line parameters pressure-broadening coefficient and pressure-induced shift. Parameters for each individual line were fitted using multiple laboratory spectra simultaneously. Relative line intensities were also fitted but strictly constrained to the Margolis (1988) values given in HITRAN, permitting only small deviations.

Details about the multispectrum fitting technique and its advantages can be found in Benner et al. (1995). Even though the multispectrum approach greatly reduced uncertainty in the retrieval, the inverse problem remained underdetermined as the blended lines could not be fully separated. For this reason, we added additional constraints using the Optimal Estimation technique (Rodgers, 2000). This approach allowed us to attribute prior uncertainties to the target parameters, thereby minimising oscillations of parameters whose retrieval errors would be strongly correlated in an unconstrained least squares approach. The solution to this nonlinear constrained least squares approach which maximises the a posteriori probability density function of the state vector is given by Rodgers (2000):

$$\boldsymbol{x}_{i+1} = \boldsymbol{x}_a + \left(\mathbf{K}_i^T \mathbf{S}_\epsilon^{-1} \mathbf{K}_i + \mathbf{S}_a^{-1}\right)^{-1} \mathbf{K}_i^T \mathbf{S}_\epsilon^{-1} \cdot [\boldsymbol{y} - \boldsymbol{F}(\boldsymbol{x}_i) + \mathbf{K}_i(\boldsymbol{x}_i - \boldsymbol{x}_a)] \,, \quad (1)$$

where

$\boldsymbol{x}_a =$ a priori state vector,
$\boldsymbol{x}_i =$ state vector at the ith iteration,
$\mathbf{S}_\epsilon =$ (pixel)error covariance matrix,
$\mathbf{S}_a =$ a priori covariance matrix,
$\boldsymbol{F}(\boldsymbol{x}_i) =$ forward model evaluated at $\boldsymbol{x}_i$,
$\mathbf{K}_i =$ Jacobian of the forward model at $\boldsymbol{x}_i$,
$\boldsymbol{y} =$ measurement vector.

In our particular case the state vector comprised relative line intensity, pressure broadening parameter and pressure-induced shift of each individual line as well as a low order polynomial (for each spectrum separately) to account for broad-band baseline structures. The forward model simulates the transmission spectra of the gas cells depending on the integrated column density of methane (fixed, equals concentration c times absorption path length l) and the spectral parameters to be retrieved:

$$\boldsymbol{F}_j(\nu) = (a_{0,j} + a_{1,j}\nu) \cdot f_{\mathrm{ILS}}(\nu) \otimes \exp\left(-\sum_i S_i \cdot c_j \cdot l \cdot f_{\mathrm{voigt},\gamma_i}(\nu - \delta_i \cdot \frac{p}{p_{\mathrm{ref}}} - \nu_{0,i}\right) \quad (2)$$

where f_{ILS} is the instrumental line-shape (in our case a sinc convolved with a box function) and $\otimes$ denotes convolution. S_i,γ_i and δ_i are line intensity, N_2-broadening coefficient and pressure shift, respectively, for each transition i. f_{voigt} denotes a Voigt function and $\nu_{0,i}$ is the vacuum wave number of transition i. The entire forward model $\boldsymbol{F}$ consists of a concatenation of all j simulated transmission spectra. The entire state vector comprises S_i,γ_i and δ_i for each line i and 2 polynomial coefficients a for each spectrum j separately.

Table 1. Laboratory measurement conditions for the FTS methane spectra. FTS optical path difference was 90 cm and gas cell length 140 cm, traversed twice for the measurement.

CH_4 mixing ratio [%]	Temperature [K]	total pressure at start [hPa]	
		at start of scan	increase during scan [%]
≈ 1.2	295.65	900.0	0.1
≈ 2	295.65	500.0	0.2
≈ 2	296.15	239.9	0.2
≈ 2	297.15	125.7	0.6

Each line is treated separately, even for multiplets, and no cross-correlations between lines is assumed (i.e. $\mathbf{S}_a$ is diagonal). A standard Voigt line-shape is applied and the Jacobian of the transmission with respect to shift and broadening coefficients computed analytically, as explained in Schreier (1992) and references therein. Self-broadening was neglected since the methane volume mixing ratio in the cell was 2% at most.

From a measurement perspective, no attempt was made to determine an accurate total methane content in the cell a priori. Hence, the integrated column density of methane was determined using a fit covering the isolated R0 and R1 transitions. The line strengths retrieved in this study are thereby linked to the R0 and R1 strengths given in HITRAN (Margolis, 1988). For the final determination of spectral parameters, cell column densities were kept fixed. Prior line strengths were taken from HITRAN and prior pressure shifts are all reset to –0.011 cm^{-1} atm^{-1} as Kapitanov et al. (2007) reports this pressure shift for the R3 triplet.

Prior broadening coefficients were not taken from HITRAN but adapted from measurements in the fundamental by Pine (1992, 1997), as done by Washenfelder et al. (2003). The actual fitting was performed in 10 cm^{-1} bins for the sake of computational efficiency. In the inversion, four N_2 broadened spectra at different pressures at room temperature were used (see Table 1). As we were mainly interested in broadening coefficients, we applied relatively strict prior constraints for line intensity and pressure shift. We then performed retrievals with increasingly stricter constraints on pressure broadening and found that only for prior covariances below about $(0.002\,cm^{-1}\,atm^{-1})^2$, fit residuals started getting worse. Hence we chose this value as optimal constraint on pressure broadening. Depending on the spectral microwindow, the fit typically converged within 3–10 iterations. Table 2 lists the employed prior uncertainties for the individual parameters.

Table 2. Fit parameters used in the inversion.

relative line intensity	prior 1σ of δ_{N_2} [cm^{-1} atm^{-1}]	γ_{N_2} [cm^{-1} atm^{-1}]
0.1%	0.001	0.002

4 Results and discussion

Figures 2, 3 and 4 show the fit results for the P, Q and R-branch, respectively. Only measured FTS spectra and fitting residuals are displayed. As can be seen in the systematic red residuals, applying the HITRAN database yields wrong linewidths and partly shifted lines. While there only seems to be a shift for low rotational levels in the Q branch, higher levels show systematic residuals typical of too high broadening coefficients (wings too strong, line center too weak). The P and R-branches behave similarly and a zoom on the R6 multiplet in Fig. 5 shows the improvements in the fits more clearly. Looking closely at the R6 multiplet, some systematic residuals at intermediate pressures (125 and 250 hPa) exist, hinting at deviations from the Voigt line-shape, perhaps due to Dicke-narrowing. Line-mixing as observed in the ν_3 fundamental can also play a role. The same holds true for other transitions. However, those residuals are typically below 1%, being very small compared to residuals induced when applying the current HITRAN broadening coefficients. Overall, the final residuals after fitting line parameters show far less systematic features and are dominated by the instrumental artifact of channeling due to the applied spectral filter.

The fitted N_2 broadening coefficients and pressure shifts for strong transitions in the spectral region under investigation are shown in Fig. 6, along with the ratio of present and HITRAN line strengths. To estimate possible systematic errors and the impact of prior values in the retrieved parameters, additional fits were performed with varying assumptions as a sensitivity study:

- 2 fits with different low frequency correction terms for the channeling;
- 1 fit where methane abundances in the cell are an additional fit parameter, i.e. not fixed;
- 1 fit with HITRAN broadening and pressure shift parameters as prior;
- 2 fits with universal prior values for pressure-broadening: 0.058 and 0.05 cm^{-1} atm^{-1}.

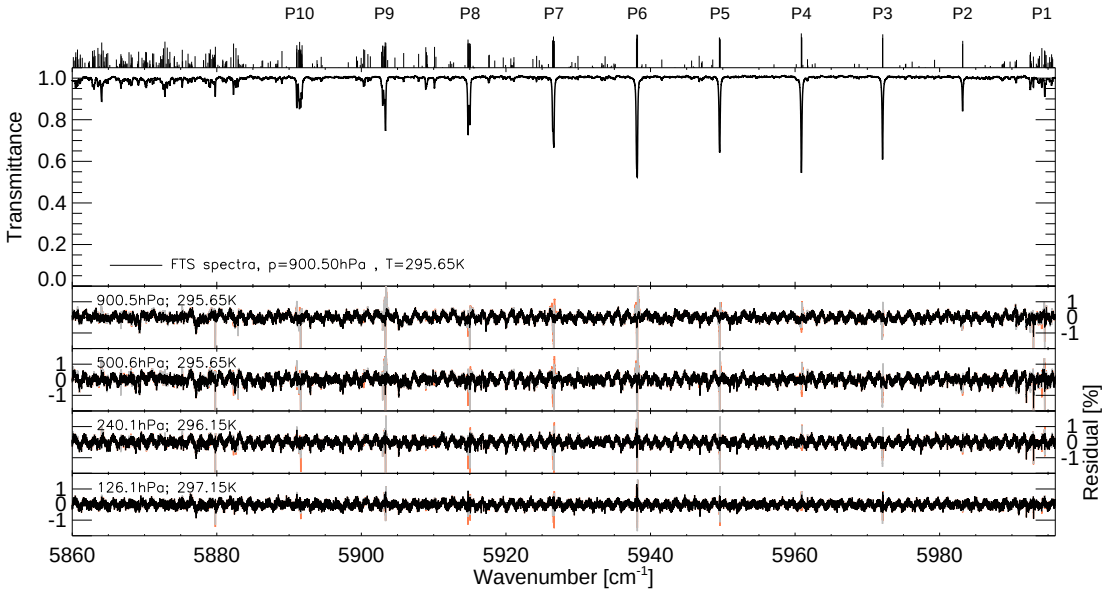

Fig. 2. Fit results of the multi-spectra inversion for the P-branch. The upper panel depicts the N_2 broadened FTS spectrum at 900.5 hPa. The lower panels show the fitting residuals for each FTS spectrum (decreasing pressure from top to bottom) separately in black (measured-modelled times 100). The red lines indicate residuals if no changes to the HITRAN database were applied. The gray lines show residuals using the HITRAN database but replacing broadening coefficients with results by Pine (1992, 1997) in the fundamental.

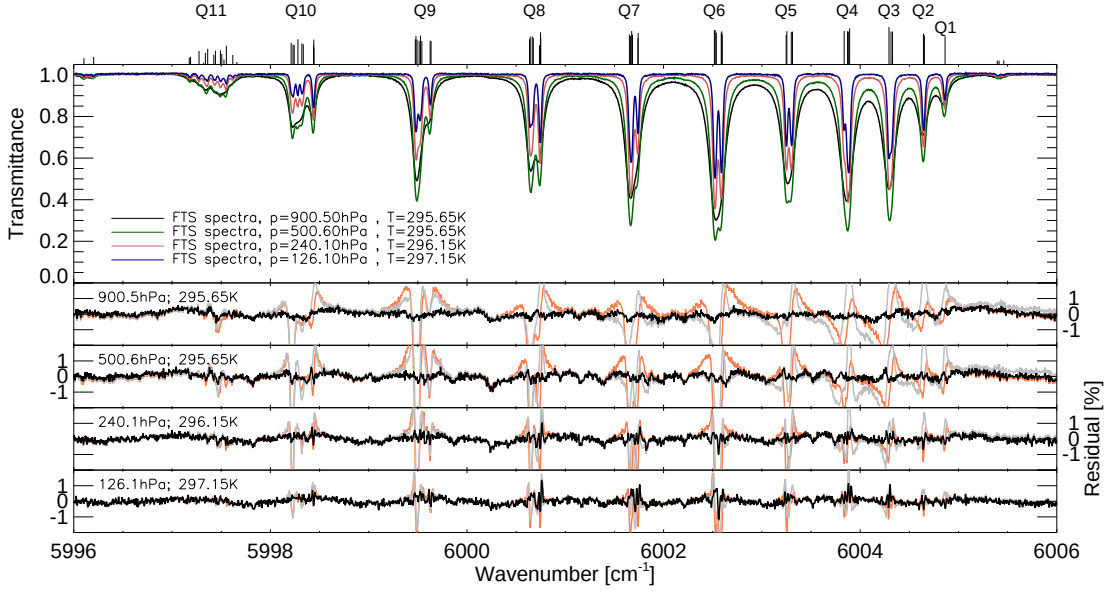

Fig. 3. As in Fig. 2 but for the Q-branch and with all FTS spectra plotted in the upper panel (black: 900.5 hPa; green:500.6 hPa; red:240.1 hPa; blue:126.1 hPa)

Table 3 gives an overview of the results for the transitions of the $2\nu_3$ band that are assigned in HITRAN (please note that some upper state rotational levels are not yet attributed to specific transitions). The outcome of the sensitivity study is used as an error estimate for retrieved broadening coefficients and pressure shifts.

For isolated lines, such as R0 and R1, the retrieval is very stable and insensitive to prior assumptions; accuracies are expected to be about 1%. Larger variations occur when lines are strongly blended as spectral parameters within multiplets are underdetermined, deteriorating accuracies to about 5–10%. However, even for those transitions we did not find

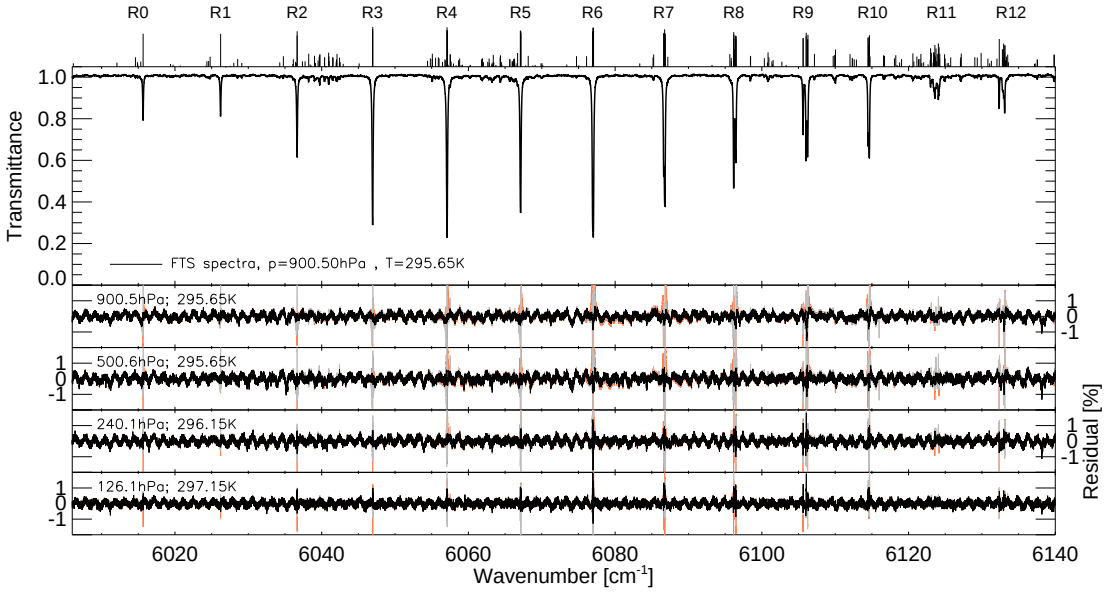

Fig. 4. As in Fig. 2 but for the R-branch.

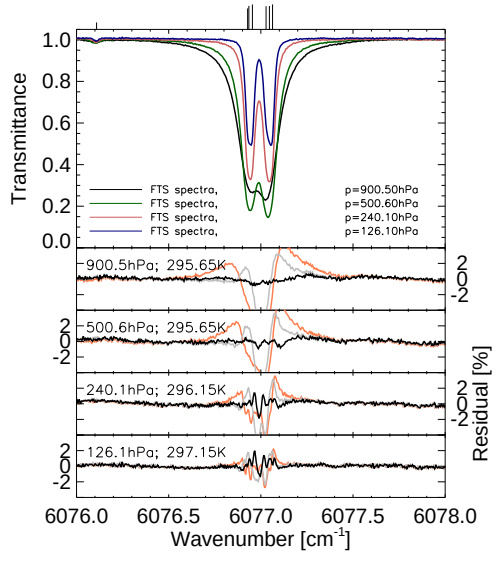

Fig. 5. As in Fig. 3 but for the R6 manifold with six strong transitions. The sum of the measured intensities in the manifold is greater by only 1.2% compared to the Margolis (1988) values. In contrast, the average of measured widths is 19% smaller than the average of default widths applied in HITRAN. The residuals seen in the fit of the lowest pressure spectrum could arise from combined inaccuracies of the retrieved positions, relative strengths, widths, the presence of weak transitions not included in the database or effects of non-Voigt line-shapes.

a systematic dependence on the prior. Figure 7 shows the retrieved broadening parameters as a function of |m|, where |m| corresponds to the rotational state J (upper state J for R branch lines, lower state for the Q and P-branch). The |m| dependence is very similar for all branches, slightly increasing in the beginning with decreasing widths for higher rotational levels. As for the comparison with results from the ν_3 band (Pine, 1992, 1997), which are displayed in the lower panel, we see a slightly different |m| dependence, especially at higher rotational levels our measurements show systematically lower broadening coefficients. Pine (1992, 1997) included collisional narrowing in their analysis and broadening parameters derived with a non-Voigt profile cannot be easily compared with Voigt-only retrievals, as can be seen in Dufour et al. (2003). However, Predoi-Cross et al. (2006) noted similar differences at higher J in the air-broadened widths at 4300 cm^{-1}. Finally, at the end of the present study, new measurements of N_2-broadening in the ν_4 fundamental were reported by Martin and Lepère (2008). Comparison for 31 transitions with the same rotational quantum assignments produced an average ratio (ν_4 to $2\nu_3$ widths) of 1.01±13%. Given the experimental precisions of the studies, the large root-mean-square is interpreted as evidence of the vibrational dependences of the widths, as discussed by Predoi-Cross et al. (2006). However, such conclusions must await theoretical validation through the calculations such as those produced by Antony et al. (2008).

One should mention that it is virtually impossible to derive independent spectral parameters within a multiplet, especially in the congested Q-branch. Errors in the retrieved parameters are therefore strongly correlated and differences

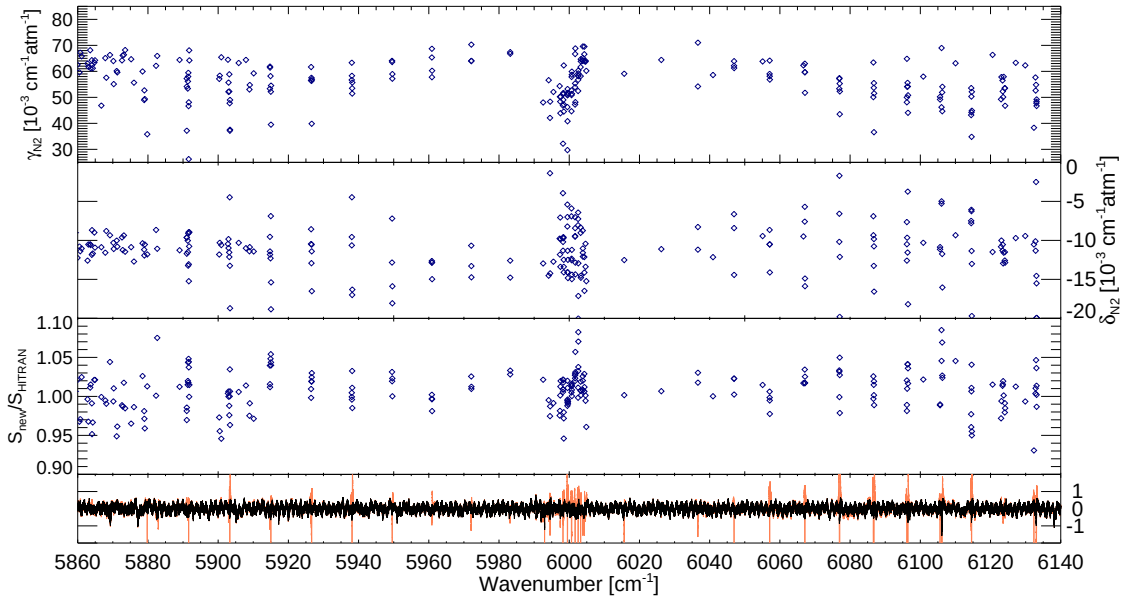

Fig. 6. N_2-broadening coefficients (upper panel, in $10^{-3}\,cm^{-1}\,atm^{-1}$), pressure shifts (middle panel, in $10^{-3}\,cm^{-1}\,atm^{-1}$) and ratio of present line intensities compared to HITRAN (lower panel, mean ratio=1.013) retrieved for all transitions with line intensities above $5{\cdot}10^{-23}\,cm^{-1}/(molecule\,cm^{-2})$. The lowest panel again depicts fitting residuals (black line) and residuals assuming HITRAN parameters (red) for the 900 hPa spectra.

in retrieved broadening coefficients within a multiplet should be interpreted with care as many solutions can lead to identical line-shapes. For example, different retrieved pressure shifts within a multiplet might accommodate line-mixing or Dicke narrowing features, thereby not representing the pressure shift in its physical sense any more. However, the main objective of this work is to create a set of empirical spectroscopic parameters that allows a best possible modelling of methane cross sections at typical pressures encountered in the Earth's atmosphere applying the simple and widely-used Voigt line-shape.

There are only a few studies of broadening parameters in the $2\nu_3$ band to compare with and a comparison for multiplets is not straightforward as the results depend on a variety of assumptions that might differ from study to study. However, for the fully isolated R0 and R1 lines a comparison is possible with work from Darnton and Margolis (1973) and also with the results from Pine (1997) for the fundamental. The comparison is shown in Table 4 and shows very good agreement between the different results, both in absolute terms and also concerning the difference of the broadening coefficient between the R0 and R1 line.

4.1 Open issues

Studies of methane pressure broadening are greatly hindered by the lack of basic characterization of the spectrum in this region. The spectral interval between 4800 and 6300 cm^{-1} contains 14 vibrational bands with some 60 sub-vibrational components. A complete linelist would likely contain more than 20,000 features, but at present no global analysis has been published to provide a reliable calculation of line positions, strengths and lower state energies. Similarly, there is no theoretical model that predicts pressure broadening coefficients with the accuracies required for state-of-the-art remote sensing. Hence, more laboratory measurements and development of theoretical models are needed to achieve 1% accuracies for line intensities and broadening parameters as well as to resolve line-mixing and collisional-narrowing effects.

Temperature dependence of pressure broadening is so far unknown for most transitions and therefore requires further research. While HITRAN attributes a temperature exponent of 0.75 universally in the spectral range considered here, Darnton and Margolis (1973) and Gharavi and Buckley (2005) find values ranging between 0.83 and 0.93 for R0-R4 in the $2\nu_3$ branch. At 243 K, this might already lead to discrepancies in the broadening coefficient of 3% (temperature exponent 0.75 vs 0.9). The theoretical prediction in a recent study by Antony et al. (2008) may provide some guidance about the variation of the temperature dependence as a function of the quantum numbers. In any case, atmospheric scientists using the HITRAN database should thus be aware of its uncertainties as provided in error codes and referenced original literature.

Table 3. Retrieved broadening coefficients and pressure shifts in the $2\nu_3$ band for $^{12}CH_4$ listed for lower rotational level J″, symmetry species C″ and ordering index n″. For broadening coefficients and pressure shifts, the standard deviation of the fitted parameters in the sensitivity study is provided as error estimate. The differences to HITRAN and to Pine (1992, 1997) values are listed separately, calculated as $((\gamma_{\text{this study}} - \gamma_{\text{reference}})/\gamma_{\text{reference}} * 100)$. Broadening parameters are given for 296 K, assuming a temperature dependence exponent of 0.75. A more detailed list as well as retrieved parameters for all lines are provided in the supplementary material. http://www.atmos-chem-phys.net/8/5061/2008/acp-8-5061-2008-supplement.zip

J″	C″	n″[a]	line position [cm^{-1}]	γ_{N_2} (1σ) [10^{-3} cm^{-1} atm^{-1}]	% Δ -HITRAN	% Δ -Pine(1992,1997)	δ_{N_2} (1σ) [10^{-3} cm^{-1} atm^{-1}]
P10	F	–	5891.0652	57.2 (8.8)	5.9	–	–9.6 (0.3)
P10	A2	1	5891.0676	54.2 (5.7)	0.4	6.1	–9.6 (0.5)
P10	E	–	5891.0695	37.2 (10.)	–31.1	–	–11.7 (1.0)
P10	F	–	5891.3418	53.4 (1.1)	–1.1	–	–10.0 (0.7)
P10	F	–	5891.3784	56.1 (1.3)	3.9	–	–11.4 (0.8)
P10	A1	1	5891.4572	58.0 (0.5)	7.4	3.3	–13.2 (0.3)
P10	F	–	5891.5008	59.4 (1.5)	10.0	–	–9.1 (0.9)
P10	F1	1	5891.5826	46.7 (1.6)	–13.5	–17.9	–8.9 (1.2)
P10	E	1	5891.6159	26.2 (1.8)	–51.4	–27.5	–13.0 (0.6)
P10	F2	1	5891.6452	48.1 (1.5)	–10.9	–15.6	–15.2 (0.7)
P9	F	–	5902.9488	52.1 (0.6)	–10.1	–	–9.8 (0.5)
P9	F	–	5902.9645	55.7 (0.9)	–4.0	–	–10.9 (0.5)
P9	F	–	5903.1035	59.5 (3.3)	2.6	–	–11.2 (1.1)
P9	E	–	5903.1591	52.3 (1.1)	–9.8	–	–11.5 (0.7)
P9	F	–	5903.1800	58.9 (1.1)	1.6	–	–12.1 (0.6)
P9	A1	1	5903.2861	47.7 (0.4)	–17.7	–15.9	–4.4 (0.4)
P9	F	–	5903.3376	37.2 (1.0)	–35.8	–	–13.2 (1.0)
P9	F	–	5903.3654	37.6 (1.9)	–35.1	–	–22.9 (0.5)
P9	A2	1	5903.3857	49.0 (0.6)	–15.5	–14.5	–18.7 (1.0)
P8	A1	1	5914.7515	53.3 (1.1)	–8.1	0.2	–9.5 (0.7)
P8	F1	2	5914.7651	61.9 (5.0)	6.7	7.9	–11.4 (0.5)
P8	E	2	5914.7762	61.5 (1.9)	6.0	9.8	–11.8 (0.9)
P8	F2	2	5914.9181	58.2 (0.6)	0.3	–1.0	–12.2 (0.3)
P8	F1	1	5915.0006	52.2 (0.5)	–10.0	–15.4	–6.8 (0.4)
P8	E	1	5915.0461	39.5 (0.9)	–31.8	–18.2	–18.8 (0.4)
P8	F2	1	5915.0631	54.5 (0.6)	–6.0	–8.2	–15.3 (0.5)
P7	F2	1	5926.4662	56.5 (0.3)	–11.7	–11.2	–10.4 (0.4)
P7	F1	1	5926.4837	61.7 (0.9)	–3.6	2.2	–8.5 (0.3)
P7	A2	1	5926.5755	57.6 (0.2)	–10.0	–2.8	–12.9 (0.2)
P7	F2	2	5926.6250	56.4 (0.6)	–11.8	–8.4	–10.5 (0.8)
P7	E	1	5926.6482	39.9 (1.1)	–37.6	–16.2	–11.4 (0.4)
P7	F1	2	5926.6785	57.0 (0.4)	–10.9	–3.7	–16.5 (0.3)
P6	E	1	5938.0571	56.7 (0.8)	–11.4	–6.9	–10.6 (0.4)
P6	F2	2	5938.0661	63.3 (1.1)	–1.1	–1.6	–9.5 (0.2)
P6	A2	1	5938.0947	58.3 (0.3)	–8.9	–4.9	–4.4 (0.2)
P6	F2	1	5938.1676	53.5 (0.4)	–16.4	–18.8	–16.9 (0.6)
P6	F1	1	5938.1901	51.5 (1.1)	–19.5	–18.6	–21.3 (0.3)
P6	A1	1	5938.2086	55.7 (0.1)	–12.9	–6.5	–16.3 (0.5)
P5	F1	1	5949.5276	64.1 (0.2)	–2.9	2.9	–12.8 (0.4)
P5	F2	1	5949.5526	63.6 (0.6)	–3.6	–5.0	–7.1 (0.2)
P5	F1	2	5949.6100	57.2 (0.9)	–13.3	–11.6	–18.0 (0.3)
P5	E	1	5949.6214	59.0 (0.9)	–10.6	3.1	–15.8 (0.5)

[a] Transitions for which the n″ are not shown are thought to be perturbed and may in fact be a different assignment altogether. In addition, some of the assigned transitions may be blended with transitions from other bands. A full analysis of the bands in this region is needed before an accurate interpretation of the measurements can be made.

Table 3. Continued.

J″	C″	n″[a]	line position [cm^{-1}]	γ_{N_2} (1σ) [10^{-3} cm^{-1} atm^{-1}]	% Δ -HITRAN	% Δ -Pine(1992,1997)	δ_{N_2} (1σ) [10^{-3} cm^{-1} atm^{-1}]
P4	A1	1	5960.8670	65.4 (0.2)	–0.9	–0.1	–12.6 (0.6)
P4	F1	1	5960.8837	68.7 (2.1)	4.1	0.0	–12.8 (0.7)
P4	E	1	5960.8975	57.8 (1.4)	–12.4	–3.6	–12.8 (0.8)
P4	F2	1	5960.9339	60.3 (0.3)	–8.6	–4.5	–14.9 (0.3)
P3	F1	1	5972.0960	64.0 (0.5)	–3.0	–6.3	–10.6 (0.7)
P3	F2	1	5972.1136	70.3 (2.1)	6.5	4.2	–13.2 (0.4)
P3	A2	1	5972.1347	64.1 (0.2)	–2.9	2.2	–14.7 (0.5)
P2	E	1	5983.1839	67.4 (1.7)	2.1	1.9	–12.5 (0.4)
P2	F2	1	5983.1942	66.8 (0.4)	1.2	1.7	–14.7 (0.4)
P1	F1	1	5994.1451	56.6 (0.9)	–14.2	–4.8	–14.5 (0.4)
Q10	F	–	5998.2112	46.8 (0.7)	–13.3	–	–3.9 (1.3)
Q10	F	–	5998.2304	32.2 (1.5)	–40.3	–	–10.1 (0.4)
Q10	F	–	5998.2426	51.2 (1.9)	–5.2	–	–11.3 (0.8)
Q10	A1	1	5998.2804	51.4 (0.8)	–4.8	–7.1	–9.7 (0.4)
Q10	F	–	5998.3198	49.0 (1.3)	–9.3	–	–9.5 (0.6)
Q10	F	–	5998.3348	51.7 (1.3)	–4.3	–	–9.6 (1.0)
Q10	F	–	5998.4396	62.3 (11.)	15.4	–	–13.3 (0.7)
Q10	A2	1	5998.4419	44.5 (2.6)	–17.5	–11.4	–14.0 (0.7)
Q10	E	2	5998.4427	47.3 (10.)	–12.4	–5.8	–12.4 (0.7)
Q9	F2	2	5999.4743	51.0 (2.6)	–12.0	–5.2	–8.2 (0.6)
Q9	A2	1	5999.4810	46.3 (1.1)	–20.1	–23.4	–5.4 (1.2)
Q9	F1	3	5999.4921	29.7 (1.3)	–48.7	–42.1	–7.0 (0.8)
Q9	F1	2	5999.5138	40.8 (3.6)	–29.6	–31.2	–14.0 (0.7)
Q9	A1	1	5999.5270	53.2 (0.9)	–8.27	–10.0	–14.0 (1.1)
Q9	E	1	5999.5410	50.9 (1.4)	–12.2	–2.7	–11.3 (0.5)
Q9	F2	1	5999.6254	51.4 (0.7)	–11.3	–15.9	–12.4 (0.5)
Q9	F1	1	5999.6343	51.8 (1.2)	–10.6	–18.3	–14.8 (0.3)
Q8	E	1	6000.6368	52.7 (5.5)	–9.1	5.2	–6.9 (1.3)
Q8	F2	1	6000.6434	44.7 (2.5)	–22.9	–25.7	–5.9 (1.0)
Q8	F1	1	6000.6635	50.9 (2.2)	–12.2	–19.7	–12.5 (1.0)
Q8	F2	2	6000.6749	57.9 (1.7)	–0.2	–1.0	–12.3 (0.9)
Q8	E	2	6000.7373	59.9 (6.4)	3.3	3.5	–11.2 (1.0)
Q8	A1	1	6000.7484	51.4 (2.2)	–11.3	–4.6	–14.9 (0.2)
Q8	F1	2	6000.7507	58.7 (3.8)	1.2	2.5	–14.3 (0.4)
Q7	F2	2	6001.6524	53.9 (0.9)	–15.7	–13.0	–7.0 (1.3)
Q7	F1	2	6001.6646	47.2 (3.1)	–26.2	–20.9	–9.5 (0.4)
Q7	A2	1	6001.6752	55.4 (1.6)	–13.4	–7.3	–9.4 (1.3)
Q7	F1	1	6001.6841	66.7 (3.3)	4.2	6.9	–8.4 (0.5)
Q7	E	1	6001.7389	48.2 (6.5)	–24.6	–4.2	–12.8 (0.5)
Q7	F2	1	6001.7416	68.8 (5.0)	7.5	5.0	– 14.3 (0.6)
Q6	A	–	6002.5172	58.4 (1.4)	–8.8	–	–8.0 (0.5)
Q6	F	–	6002.5253	52.5 (1.8)	–17.9	–	–7.2 (0.4)
Q6	F	–	6002.5367	56.7 (0.9)	–11.4	–	–6.4 (0.6)
Q6	F	–	6002.5862	59.2 (2.4)	–7.5	–	–20.0 (0.6)
Q6	A	–	6002.5922	60.3 (4.3)	–5.8	–	–17.1 (0.3)
Q6	E	–	6002.5969	58.2 (3.7)	–9.1	–2.9	–12.9 (0.7)
Q5	E	1	6003.2472	61.7 (5.6)	–6.5	6.0	–8.3 (0.9)
Q5	F1	2	6003.2540	58.2 (2.6)	–11.8	–10.8	–9.0 (0.5)
Q5	F2	1	6003.2987	64.7 (1.2)	–2.0	–6.2	–14.5 (0.2)
Q5	F1	1	6003.3111	63.8 (0.4)	–3.3	–2.0	–14.7 (0.5)

Table 3. Continued.

J″	C″	n″[a]	line position [cm^{-1}]	γ_{N_2} (1σ) [10^{-3} cm^{-1} atm^{-1}]	% Δ -HITRAN	% Δ -Pine(1992,1997)	δ_{N_2} (1σ) [10^{-3} cm^{-1} atm^{-1}]
Q4	F2	1	6003.8370	64.0 (0.1)	–3.0	–2.9	–8.7 (0.2)
Q4	F1	1	6003.8714	64.3 (1.7)	–2.6	–5.8	–11.5 (0.7)
Q4	E	1	6003.8830	65.1 (4.8)	–1.4	5.8	–11.0 (0.3)
Q4	A1	1	6003.8928	69.6 (1.7)	5.5	4.3	–12.0 (0.7)
Q3	A2	1	6004.2930	66.6 (0.2)	0.9	4.1	–12.1 (0.4)
Q3	F1	1	6004.3133	69.5 (1.7)	5.3	0.0	–14.1 (0.3)
Q3	F2	1	6004.3291	63.9 (0.5)	–3.2	–0.1	–16.4 (0.6)
Q2	F2	1	6004.6435	63.8 (0.4)	–3.3	–2.4	–10.4 (0.2)
Q2	E	1	6004.6527	64.1 (0.8)	–2.9	1.4	–13.3 (0.2)
Q1	F1	1	6004.8632	60.2 (0.3)	–8.8	–5.5	–15.2 (0.1)
R0	A1	1	6015.6643	59.1 (0.1)	–10.4	0.9	–12.5 (0.2)
R1	F1	1	6026.2274	64.4 (0.2)	–2.4	–0.1	–11.1 (0.0)
R2	E	1	6036.6536	54.2 (2.3)	–17.8	–7.9	–8.2 (0.2)
R2	F2	1	6036.6584	71.0 (1.9)	7.6	6.2	–11.1 (0.2)
R3	F2	1	6046.9420	62.1 (2.1)	–5.9	–6.3	–6.6 (0.5)
R3	F1	1	6046.9527	63.9 (3.6)	–3.2	–5.5	–8.4 (0.1)
R3	A2	1	6046.9647	61.3 (1.7)	–7.1	3.1	–14.4 (0.2)
R4	E	1	6057.0778	59.0 (1.5)	–10.6	7.8	–8.6 (0.3)
R4	A1	1	6057.0861	64.2 (2.0)	–2.7	7.4	–10.4 (0.5)
R4	F1	1	6057.0998	58.1 (1.5)	–11.9	–13.9	–10.5 (0.5)
R4	F2	1	6057.1273	56.8 (0.2)	–13.9	–9.2	–14.1 (0.3)
R5	F2	1	6067.0816	59.7 (0.2)	–9.5	–7.2	–7.5 (0.1)
R5	F1	1	6067.0997	63.0 (0.4)	–4.5	1.4	–5.6 (0.1)
R5	E	1	6067.1485	51.8 (0.6)	–21.5	–4.3	–14.8 (0.1)
R5	F1	2	6067.1570	59.7 (0.3)	–9.5	–1.6	–15.8 (0.2)
R6	E	1	6076.9280	53.3 (0.9)	–16.7	–4.4	–10.1 (0.3)
R6	F2	2	6076.9350	57.2 (0.6)	–10.6	–8.1	–6.5 (0.0)
R6	A2	1	6076.9540	57.4 (0.2)	–10.3	–0.1	–1.7 (0.1)
R6	F1	1	6077.0283	55.3 (0.7)	–13.5	–10.5	–19.8 (0.5)
R6	F2	1	6077.0466	43.5 (0.9)	–32.0	–31.6	–21.9 (0.2)
R6	A1	1	6077.0636	52.3 (0.1)	–18.2	–11.1	–12.1 (0.3)
R7	F1	1	6086.6229	50.1 (0.3)	–21.7	–16.4	–6.9 (0.2)
R7	F2	1	6086.6350	63.4 (0.6)	–0.9	0.9	–9.3 (0.1)
R7	A2	1	6086.7454	53.7 (0.1)	–16.0	–0.0	–13.2 (0.1)
R7	F2	2	6086.7797	55.5 (0.5)	–13.2	–6.0	–9.8 (0.5)
R7	E	1	6086.7994	36.6 (0.7)	–42.8	–15.4	–10.7 (0.1)
R7	F1	2	6086.8307	51.5 (0.2)	–19.5	–6.7	–16.5 (0.2)
R8	F1	2	6096.1665	48.1 (1.2)	–17.0	–17.0	–7.6 (0.3)
R8	A1	1	6096.1743	50.0 (1.9)	–13.7	2.6	–12.5 (0.7)
R8	E	2	6096.1809	64.8 (5.6)	11.7	21.1	–10.4 (0.6)
R8	F2	2	6096.3727	55.6 (0.1)	–4.1	0.7	–11.5 (0.1)
R8	F1	1	6096.4244	54.2 (0.1)	–6.6	–7.6	–3.7 (0.2)
R8	E	1	6096.4856	44.1 (0.5)	–23.9	–7.8	–21.5 (0.3)
R8	F2	1	6096.5015	50.8 (0.3)	–12.4	–14.5	–18.1 (0.2)
R9	F1	1	6105.6259	50.2 (4.4)	–13.4	–13.2	–10.8 (0.6)
R9	F2	1	6105.6261	49.2 (5.6)	–15.1	–14.0	–11.1 (0.9)
R9	F	–	6106.0402	46.2 (1.1)	–20.3	–	–5.2 (0.4)
R9	A1	1	6106.0505	69.0 (1.1)	19.0	28.5	–4.9 (0.2)
R9	E	–	6106.1943	52.7 (7.7)	–9.1	–	–17.1 (1.4)
R9	F1	3	6106.2205	51.9 (0.4)	–10.5	7.2	–11.7 (0.6)
R9	F2	2	6106.2520	44.7 (0.7)	–22.9	–16.9	–25.1 (0.2)
R9	A2	1	6106.2841	54.1 (0.1)	–6.7	–6.3	–16.0 (0.1)

Table 4. Comparison of retrieved R0 and R1 N_2-broadening coefficients with literature.

line	This study	Darnton and Margolis (1973)	Pine (1997) (ν_3)
R0	59.1 ($\pm$0.2(2σ))	59.0 ($\pm$06.7(1σ))	58.7 ($\pm$0.17(1σ))
R1	64.4 ($\pm$0.4(2σ))	63.7 ($\pm$10.2(1σ))	64.7 ($\pm$0.08(1σ))

4.2 Additional information

Along with the results described in the paper, we provide two files with supplementary information http://www.atmos-chem-phys.net/8/5061/2008/acp-8-5061-2008-supplement.zip. One file lists retrieval results (line strengths, broadening coefficients and pressure induced shifts) and associated standard deviations from the sensitivity studies for about 1300 lines in the 5860 to 6184.5 cm^{-1} range. A second file provides these results in a HITRAN-format (2001) file for easy application. In this file, the following changes were made:

- retrieved N_2-broadening coefficients are scaled with 0.985 to give an estimate of air-broadening;
- empirical lower state energies measured by Margolis (1990) are restored;
- exponent of the temperature dependence of broadening has been reset to 0.85 for all lines;
- default value for shifts are changed from –0.008 to –0.011 cm^{-1} atm^{-1} at 296 K.

Even though the results of this study are most reliable for almost 150 strong lines of the $2\nu_3$ band, about 1300 transitions in the considered spectral range have been fitted and the results incorporated in the supplementary files http://www.atmos-chem-phys.net/8/5061/2008/acp-8-5061-2008-supplement.zip.

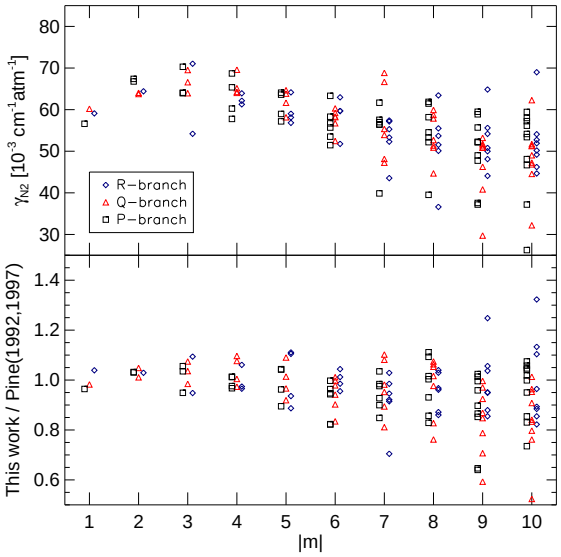

Fig. 7. Measured N_2-broadening coefficients retrieved in the P, Q and R-branch (depicted as black square, red triangle, blue diamond, respectively) as a function of |m|, where |m| is the lower state J for P and Q transitions and the upper state J for R branch lines. For easier identification, branches are slightly shifted with respect to |m|. The lower panels depicts the ratio of the retrievals with results from Pine (1992, 1997) in the ν_3 band. Values greater than one indicate that broadening coefficients retrieved in this study are larger than those from Pine (1992, 1997)

5 Impact on atmospheric methane measurements

Erroneous broadening coefficients can have a profound impact on the retrieval of gases (Washenfelder et al., 2003). Mondelain et al. (2007) found deviations of up to 7% due to line-mixing and pressure broadening effects in atmospheric profile retrievals. In this study we consider total column retrievals which should be less susceptible to errors in lineshapes as compared to profile retrievals that actually rely on an accurate knowledge of the line-shape to differentiate trace gas perturbations at different height layers. However, possible errors depend on a variety of factors like spectral resolution, retrieval method and viewing geometry.

Here we discuss two kinds of measurements, first a high resolution ground based direct sun measurement using an FTIR instrument located in Bremen, Germany, and second retrievals from the SCIAMACHY instrument (Bovensmann et al., 1997) onboard the European research satellite ENVISAT. As SCIAMACHY retrievals are the main driver for this study, we focus only on the Q and R-branch in both cases.

As pure nitrogen was used as foreign gas in the laboratory measurements, retrieved broadening coefficients need to be converted for atmospheric applications. Pine (1992) finds a relatively constant mean pressure broadening ratio of 0.937 for O_2 compared to N_2. Hence we scale the retrieved N_2 broadening coefficients with 0.985 (weighted average according to atmospheric abundances) to derive air-broadening coefficients needed for the analysis of atmospheric spectra used in this section.

Table 5. FTIR methane total columns retrieved with the updated spectroscopy and HITRAN at two different solar zenith angles. The root mean square of the fit is about 0.5% using HITRAN and improves to about 0.3% using the updated spectroscopy.

time (UTC)	SZA	retrieved CH_4 column [10^{19}molec cm^{-2}]	
		updated spec	HITRAN spec
06:24	63.510	3.855	3.806
09:14	39.443	3.860	3.892

5.1 Ground based high resolution solar absorption measurements

Two ground-based solar absorption FTIR-spectra, covering the near infrared spectral region are analysed. The FTIR measurements were performed at the University of Bremen (53.1° N, 8.9° E) with a Bruker 125 HR and an optical path difference of 45 cm, corresponding to a resolution of $0.022\,\mathrm{cm}^{-1}$. As a possible retrieval bias due to erroneous broadening coefficients largely depends on the observed airmass (defined as $1/\cos(SZA)$, where SZA denotes the solar zenith angle), we analyse two spectra from 3 July 2006 at different solar zenith angles, 63.510° (Airmass=2.242, 06:24 UTC) and 39.443° (Airmass=1.295, 09:14 UTC). A fit at high solar zenith angle is shown in Fig. 8. Pressure, temperature and water vapour profiles were taken from NCEP (National Centers for Environmental Prediction), the initial CH_4 profile from a TM5 model run (similar to the S1 scenario described in Bergamaschi et al., 2007) and the CO_2 profile set to a constant 380 ppm (parts per million). We used a least squares approach and scaled the entire initial profiles with factors for the respective trace gases. A disk center solar spectrum was calculated from a linelist provided by Geoffrey Toon, Jet Propulsion Laboratory, Pasadena, USA. CO_2 spectroscopic parameters from a recent study by Toth et al. (2007) are applied.

The lower panel in Fig. 8 shows the residuals using the methane spectroscopic parameters derived in this study and the parameters given by HITRAN. It is striking that the new methane spectroscopy largely reduces systematic residual structures, not only for the methane lines itself but also for the CO_2 lines which exhibit a slight shift when HITRAN methane spectroscopy is applied. This is most likely due to the updated pressure shifts. Table 5 shows the retrieval results for the two different FTIR spectra applying updated and HITRAN methane spectroscopic parameters. As the time difference between the measurements was short (below 3 hours), the methane vertical column is expected to remain rather constant. This is true for the retrievals using the updated spectroscopy, where the difference between the two measurements is only 0.13%, underlining the precision that can be achieved in this spectral range. However, applying HITRAN spectroscopic parameters, the difference is 2.3%, rendering the retrievals virtually useless for the detection of small changes in atmospheric methane abundances. A similar systematic error depending on solar zenith angle was already found by Washenfelder et al. (2003) for the P-branch of the $2\nu_3$ band.

5.2 Low resolution space borne measurements by SCIAMACHY onboard ENVISAT

Previous studies suggest systematic biases in the SCIAMACHY methane retrievals (Frankenberg et al., 2006; Bergamaschi et al., 2007). Here we analyse the impact of the new spectroscopy using the retrieval approach described in Frankenberg et al. (2005b) for the year 2004. Two retrieval runs were performed that only differed in methane spectroscopy, all other retrieval parameters being identical. Figure 9 shows the average differences for the entire globe averaged through a year as well as latitudinal averages for individual months. The new retrieval gives in general higher methane columns, ranging from 0 to 1.5%. This can be easily explained by narrower lines that absorb less efficient as they are not resolved by SCIAMACHY (in contrast to the FTIR retrievals). Over highly elevated regions, such as the Himalayas or Andes, the differences are negligible. This can be explained by two reasons: First, the atmosphere is optically thinner, leading to less saturation effects that would be governed by line-widths. Second, pressure broadening and shift are less dominant.

The differences for North America, for example, over the Rocky Mountains are smaller compared to the eastern regions. In that particular case, wrong spectroscopic parameters would create an artificial east-west gradient. The right panel of Fig. 9 depicts the dependence of the mean latitudinal bias on season, exemplified by 4 different months. Differences are minimal in tropical regions where the solar zenith angle is low. However, at higher latitudes the solar zenith angle and thus the bias changes during the year. Artificial seasonal structures with a peak-to-peak amplitude of about 1% could thereby be generated, which is crucial for source inversions as it cannot easily be discerned from seasonally varying methane source.

The southern hemisphere, devoid of large methane sources, should exhibit a relatively small seasonal cycle and is therefore an ideal test case for the retrieval, especially since Frankenberg et al. (2006) found a distinct but unexplainable seasonal cycle in SCIAMACHY retrievals. Figure 10 shows the 30-day running mean (box filter) of SCIAMACHY retrievals over Australia in 2004. The two retrieval versions differing in spectroscopy are shown. In addition, TM5 model values optimised with accurate NOAA (National Oceanic and Atmospheric Administration) ground based flask measurements are shown (similar to model fields of scenaro S1 in Bergamaschi et al., 2007). The new version (scaled by 1.015 to match the absolute model values) corresponds very well with the model, deviating by at most by 5 parts per billion

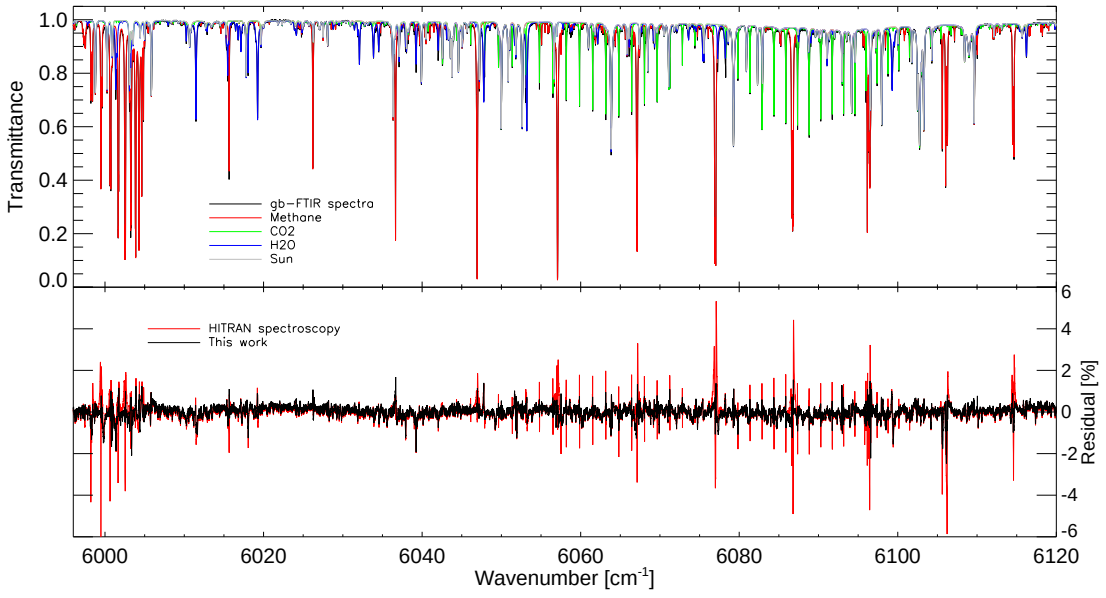

Fig. 8. Spectral fit of a ground based FTIR measurement in Bremen, Germany, measured with 45 cm optical path difference at 63.51° SZA on 3 July 2006. The upper panel shows the spectrum and the contributions of the individual gases as well as the sun (black: measured spectrum; red: Methane; green: Carbon dioxide; blue: Water vapor; grey: sun). The lower panel depicts the fit residuals (Measured-modelled) using the spectroscopic parameters from this study (black) and HITRAN(red).

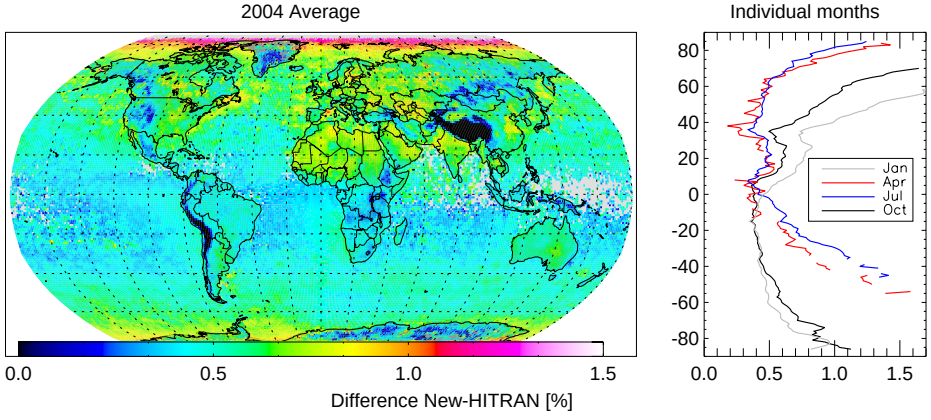

Fig. 9. Impact of spectroscopy on methane retrievals by SCIAMACHY onboard ENVISAT. The left panel shows the percentage differences averaged over the year 2004 ((xVMR CH_4(New spectroscopy) – CH_4xVMR(HITRAN spectroscopy))/CH_4xVMR(HITRAN spectroscopy)*100) on a 1 by 1 degree grid. The right panel shows the mean latitudinal differences for individual months (x-axis as in left panel; y-axis: in degree latitude).

(about 0.3%) while Frankenberg et al. (2006) found systematic seasonal biases of about 40 ppb peak to peak. Most of this previous bias is actually caused by spectroscopic interferences with water vapor, as shown by Frankenberg et al. (2008). These findings are already taken into account in this study, eliminating a large part of the seasonal bias. Using the old retrieval version (HITRAN methane spectroscopic parameters, scaled by 1.02), however, still shows a distinct deviation by about 10 ppb from April through September, corresponding with high air mass factors.

6 Conclusions

In this study, we apply a multi-spectrum fitting technique to derive N_2-broadening coefficients and pressure shifts of the methane molecule in the 5860 to 6185 cm^{-1} range which is used in methane retrievals using the SCIAMACHY spectrometer onboard ENVISAT. This range covers the strong $2\nu_3$ band for which, until now, only few transitions have been analysed with respect to pressure broadening.

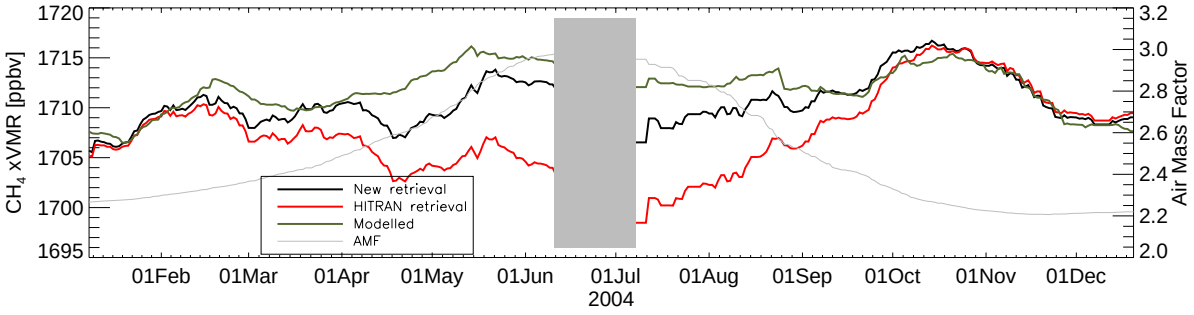

Fig. 10. Timeseries of SCIAMACHY methane column averaged mixing ratios over Australia in 2004. Concurrent CO_2 retrievals have been used as proxy for the light path (Frankenberg et al., 2005a, 2006), using CarbonTracker by NOAA for model CO_2 profiles to minimise the impact of CO_2 variations. The air mass factor is shown in grey and a decontamination period ($\pm$10 days) of the satellite is overlaid as grey box. Time series data have been smoothed with a 30-day running time-average (box filter) and spatially averaged over the entire australian continent between –20 and –30 degree latitude. Black: retrieval with new CH_4 spectroscopic parameters (this study); red: retrieval with HITRAN CH_4 spectroscopic parameters; green: modelled CH_4 mixing ratio.

Compared to the HITRAN spectroscopic database, we found systematically lower broadening parameters, especially at higher rotational levels. These results were confirmed using ground based solar absorption FTIR measurements where we found systematic residuals and biases depending on solar zenith angle when applying HITRAN spectroscopic parameters. The results of this study largely reduced residuals and the bias. Some small systematic inconsistencies between modelled and measured methane spectra still exist, probably owing to line-mixing and Dicke-narrowing effects. However, compared to the improvements achieved in this study, deviations from the Voigt line-shape are small.

We further show that SCIAMACHY retrievals based on the spectroscopy derived in this work are systematically different from a retrieval version using the HITRAN database. Differences for monthly and yearly averages are between 0 and 1.5%, depending on solar zenith angle and surface elevation. Thus, artificial seasonal structures with a peak-to-peak amplitude of about 1% can be introduced in our particular retrieval setup. With the new spectroscopy, we find only very small differences (max. 5 ppb) as compared to an atmospheric model over Australia for monthly averages.

The main purpose of this study was to provide an effective set of spectroscopic parameters for methane retrievals in the Earth's atmosphere, minimising systematic seasonal and latitudinal biases. The new spectroscopy will not only be helpful for ground-based FTIR and SCIAMACHY retrievals but also be for future space missions such as the GOSAT (Greenhouse gases Observing Satellite) mission by the Japan Aerospace Exploration Agency covering a similar spectral range for retrieval.

Acknowledgements. CF is supported by the Dutch science foundation (NWO) through a VENI grant. We acknowledge John Burrows, PI of the SCIAMACHY instrument, for having initiated the SCIAMACHY project. The experimental data for the study of the broadening parameters, used in this study, was recorded in the Molecular Spectroscopy laboratory of the Institute of Environmental Physics and Remote Sensing of the University of Bremen. This laboratory is funded by the University of Bremen and the German Aerosopsace (DLR) to undertake spectroscopic studies in support of SCIAMACHY science. We thank R. Washenfelder for providing a spectroscopic linelist based on the results of Pine et al. The Netherlands SCIAMACHY Data Center and ESA is greatly acknowledged for providing data and R. van Hees for having written the versatile NADC tools software package. We thank Jan Fokke Merink and Peter Bergamaschi for providing TM5-4DVAR methane model fields and Wouter Peters for providing CarbonTracker results. We also thank A. Segers, C. Schrijvers, and O. Tuinder for providing the ECMWF data. Part of the research described in this paper was performed at the Jet Propulsion Laboratory, California Institute of Technology, under contract with the National Aeronautics and Space Administration (NASA). We acknowledge the European Commission for supporting the 6th Framework Programme project HYMN (contract number 037048) and GEOMON (contract number 036677). We further acknowledge exchange of information within the EU 6th FP Network of Excellence ACCENT.

Edited by: W. Lahoz

References

Antony, B. K., Niles, D. L., Wroblewski, S. B., Humphrey, C. M., Gabard, T., and Gamache, R. R.: N_2, O_2 and air-broadened half-widths and line shifts for transitions in the ν_3 band of methane in the 2726–3200 cm^{-1} spectral region, Journal of Molecular Spectroscopy, 251, 268–281, 2008.

Benner, D. C., Rinsland, C. P., Devi, V. M., Smith, M. A. H., and Atkins, D.: A multispectrum nonlinear least squares fitting technique, J. Quant. Spectrosc. Radiat. Transfer, 53, 705–721, 1995.

Bergamaschi, P., Frankenberg, C., Meirink, J. F., Krol, M., Dentener, F., Wagner, T., Platt, U., Kaplan, J., Körner, S., Heimann,

M., et al.: Satellite chartography of atmospheric methane from SCIAMACHY on board ENVISAT: 2. Evaluation based on inverse model simulations, J. Geophys. Res., 112, D02304, doi:10.1029/2006JD007268, 2007.

Bovensmann, H., Burrows, J. P., Buchwitz, M., Frerick, J., Noël, S., Rozanov, V. V., Chance, K. V., and Goede, A. P. H.: SCIAMACHY: Mission Objectives and Measurement Modes, J. Atmos. Sci., 56, 127–150, 1997.

Brown, L. R., Benner, D. C., Champion, J. P., Devi, V. M., Fejard, L., Gamache, R. R., Gabard, T., Hilico, J. C., Lavorel, B., Loete, M., et al.: Methane line parameters in HITRAN, J. Quant. Spectrosc. Radiat. Transfer, 82, 219–238, 2003.

Buchwitz, M., de Beek, R., Noël, S., Burrows, J. P., Bovensmann, H., Schneising, O., Khlystova, I., Bruns, M., Bremer, H., Bergamaschi, P., Körner, S., and Heimann, M.: Atmospheric carbon gases retrieved from SCIAMACHY by WFM-DOAS: version 0.5 CO and CH_4 and impact of calibration improvements on CO_2 retrieval, Atmos. Chem. Phys., 6, 2727–2751, 2006, http://www.atmos-chem-phys.net/6/2727/2006/.

Darnton, L. and Margolis, J. S.: The temperature dependence of the half widths of some self-and foreign-gas-broadened lines of methane., J. Quant. Spectrosc. Radiat. Transfer, 13, 969–976, 1973.

Dufour, G., Hurtmans, D., Henry, A., Valentin, A., and Lepère, M.: Line profile study from diode laser spectroscopy in the $^{12}CH_4$ $2\nu_3$ band perturbed by N_2, O_2, Ar, and He, J. Mol. Spectrosc., 221, 80–92, 2003.

Frankenberg, C., Meirink, J. F., van Weele, M., Platt, U., and Wagner, T.: Assessing Methane Emissions from Global Space-Borne Observations, Science, 308, 1010–1014, doi:10.1126/science.1106644, http://www.sciencemag.org/cgi/content/abstract/308/5724/1010, 2005a.

Frankenberg, C., Platt, U., and Wagner, T.: Iterative maximum a posteriori (IMAP)-DOAS for retrieval of strongly absorbing trace gases: Model studies for CH_4 and CO_2 retrieval from near infrared spectra of SCIAMACHY onboard ENVISAT, Atmos. Chem. Phys., 5, 9–22, 2005b.

Frankenberg, C., Meirink, J. F., Bergamaschi, P., Goede, A. P. H., Heimann, M., Körner, S., Platt, U., van Weele, M., and Wagner, T.: Satellite chartography of atmospheric methane from SCIAMACHY on board ENVISAT: Analysis of the years 2003 and 2004, J. Geophys. Res., 111, D07303, doi:10.1029/2005JD006235, 2006.

Frankenberg, C., Bergamaschi, P., Butz, A., Houweling, S., Meirink, J. F., Petersen, K., Schrijver, H., Warneke, T., and Aben, I.: Tropical methane emissions: A revised view from SCIAMACHY onboard ENVISAT, Geophys. Res. Lett., 35, L15811, doi:10.1029/2008GL034300, 2008.

Gharavi, M. and Buckley, S. G.: Diode laser absorption spectroscopy measurement of linestrengths and pressure broadening coefficients of the methane $2\nu_3$ band at elevated temperatures, J. Mol. Spectrosc., 229, 78–88, 2005.

IPCC: Climate Change 2007 – The Physical Science Basis: Working Group I Contribution to the Fourth Assessment Report of the IPCC (Climate Change 2007), Cambridge University Press, Cambridge, United Kingdom and New York, NY, USA, 2007.

Kapitanov, V. A., Ponomarev, Y. N., Tyryshkin, I. S., and Rostov, A. P.: Two-channel opto-acoustic diode laser spectrometer and fine structure of methane absorption spectra in 6070–6180 cm^{-1} region, Spectrochim. Acta A, 66, 811–818, 2007.

Margolis, J. S.: Measured line positions and strengths of methane between 5500 and 6180 cm^{-1}, Appl. Opt., 27, 4038–4051, 1988.

Margolis, J. S.: Empirical values of the ground state energies for methane transitions between 5500 and 6150 cm^{-1}, Appl. Opt., 29, 2295–2302, 1990.

Martin, B. and Lepère, M.: N_2-broadening coefficients in the $\nu 4$ band of $^{12}CH_4$ at room temperature, Journal of Molecular Spectroscopy, 250, 70–74, doi:10.1016/j.jms.2008.05.001, 2008.

Mondelain, D., Payan, S., Deng, W., Camy-Peyret, C., Hurtmans, D., and Mantz, A. W.: Measurement of the temperature dependence of line mixing and pressure broadening parameters between 296 and 90K in the ν_3 band of $^{12}CH_4$ and their influence on atmospheric methane retrievals, J. Mol. Spectrosc., 244, 130–137, 2007.

Mondelain, D., Camy-Peyret, C., Deng, W., Payan, S., and Mantz, A. W.: Study of molecular line parameters down to very low temperature, Appl. Phys. B, 90, 227–233, doi:10.1007/s00340-007-2918-x, 2008.

Pine, A. S.: Self-, N_2, O_2, H_2, Ar, and He broadening in the ν_3 band Q branch of CH_4, J. Chem. Phys., 97, 773–785, 1992.

Pine, A. S.: N_2 and Ar broadening and line mixing in the P and R branches of the ν_3 band of CH_4, J. Quant. Spectrosc. Radiat. Transfer, 57, 157–176, 1997.

Pine, A. S. and Gabard, T.: Multispectrum fits for line mixing in the ν_3 band Q branch of methane, J. Mol. Spectrosc., 217, 105–114, 2003.

Predoi-Cross, A., Brawley-Tremblay, M., Brown, L. R., Malathy Devi, V., and Benner, D. C.: Multispectrum analysis of $^{12}CH_4$ from 4100 to 4635 cm^{-1}: II. Air-broadening coefficients (widths and shifts), J. Mol. Spectrosc., 236, 201–215, 2006.

Predoi-Cross, A., Unni, A. V., Heung, H., Malathy Devi, V., Benner, C. D., and Brown, L. R.: Line mixing effects in the ν_2+ ν_3 band of methane, J. Mol. Spectrosc., 246, 65–76, 2007.

Rodgers, C. D.: Inverse Methods for Atmospheric Sounding, World Scientific, London, 2000.

Rothman, L. S., Jacquemart, D., Barbe, A., Benner, D. C., Birk, M., Brown, L. R., Carleer, M. R., Chackerian, C., Chance, K., Coudert, L. H., et al.: The HITRAN 2004 molecular spectroscopic database, J. Quant. Spectrosc. Radiat. Transfer, 96, 139–204, 2005.

Schneising, O., Buchwitz, M., Burrows, J. P., Bovensmann, H., Bergamaschi, P., and Peters, W.: Three years of greenhouse gas column-averaged dry air mole fractions retrieved from satellite – Part 2: Methane, Atmos. Chem. Phys. Discuss., 8, 8273–8326, 2008, http://www.atmos-chem-phys-discuss.net/8/8273/2008/.

Schreier, F.: The Voigt and complex error function – A comparison of computational methods, J. Quant. Spectrosc. Radiat. Transfer, 48, 743–762, 1992.

Toth, R. A., Brown, L. R., Miller, C. E., Devi, V. M., and Benner, D. C.: Spectroscopic database of CO_2 line parameters: 4300-7000 cm^{-1}, J. Quant. Spectrosc. Radiat. Transfer, 109(6), 906–921, 2007.

Washenfelder, R., Wennberg, P., and Toon, G.: Tropospheric methane retrieved from ground-based near-IR solar absortion spectra, Geophys. Res. Lett., 30, 2226, doi:10.1029/2003GL017969, 2003.